Article:

Zhang, D., Rybka, G., Daw, E.J. et al. (2026) Effects of cosmic-ray muons on μeV-to-meV scale axion dark matter searches. New Journal of Physics. ISSN: 1367-2630

https://doi.org/10.1088/1367-2630/ae98a8

New Journal of Physics
The open access journal at the forefront of physics

Deutsche Physikalische Gesellschaft DPG   IOP Institute of Physics

Effects of cosmic-ray muons on μeV-to-meV scale axion dark matter searches

To cite this article before publication: Dan Zhang *et al* 2026 *New J. Phys.* in press https://doi.org/10.1088/1367-2630/ae98a8

Journal Name

Crossmark

RECEIVED
dd Month yyyy

REVISED
dd Month yyyy

PAPER

Effects of Cosmic-Ray Muons on μeV-to-meV Scale Axion Dark Matter Searches

Dan Zhang[1,*], Gray Rybka[1], Edward J. Daw[2] and Robyn Evren[2]

[1]University of Washington, Seattle, Washington 98195, USA
[2]University of Sheffield, Sheffield S10 2TN, UK
[*]Author to whom any correspondence should be addressed.

E-mail: dzhang95@uw.edu,grybka@uw.edu,e.daw@sheffield.ac.uk,revren1@sheffield.ac.uk

Keywords: cosmic-ray muon, axion haloscope, synchrotron radiation

Abstract
We estimate the synchrotron radiation emitted by cosmic-ray muons in a uniform magnetic field, focusing on the photon radiation from μeV to meV. Such events can potentially bring backgrounds to the axion dark matter searches. The GEANT4 software package is utilized to simulate the muon tracks in a cylindrical region of interest with an 8 T solenoid magnetic field applied. We further develop an analytical estimation of the angular-frequency-differential synchrotron radiation power spectra in this work as the cosmic-ray muons span a wide range of Lorentz factor γ and pitch angle α. We verify that the cosmic-ray muons are not the dominant noise background for the current axion dark matter experiments on the μeV scale because of the high quality factor Q and fine energy resolution in the readout. However, without sufficient energy resolution in the detector readout, future broadband axion dark matter experiments will be vulnerable to the synchrotron radiation of these charged particles.

1 Introduction

The Quantum chromodynamics (QCD) axion is a compelling dark matter candidate that can explain 100% of the dark matter abundance occupying 85% mass of the universe [1] and solve the strong CP problem at the same time. The so-called strong CP problem refers to the fact that CP violation is expected in the strong interaction from the QCD θ-term [2], but is never observed in the neutron electric dipole moment measurements [3, 4]. Roberto Peccei and Helen Quinn proposed a new $U(1)_{\rm PQ}$ symmetry beyond the standard model to explain the CP conservativeness in the strong interaction [5]. The QCD axion is the pseudo–Nambu–Goldstone boson after the spontaneous symmetry breaking (SSB) of the $U(1)_{\rm PQ}$ [6, 7], and can be naturally produced in the early universe through the misalignment mechanism [8, 9, 10].

When the Peccei–Quinn mechanism was first proposed, the SSB energy scale f_a of the $U(1)_{\rm PQ}$ was initially assumed to be at the electroweak scale, but this possibility was quickly ruled out by different experimental constraints [11, 12]. Stellar evolution puts a lower limit on $f_a \gtrsim 10^8$ GeV [13, 14], corresponding to the upper limit on the QCD axion mass, $m_a \lesssim 0.06$ eV. Post-inflation axion dark matter production mechanisms, including the aforementioned misalignment mechanism and topological defect decays [15, 16], strongly motivate the μeV-to-meV energy scale. Pre-inflation production with the misalignment mechanism broadens the motivated lower mass border to 0.1 μeV [9, 10], and the stochastic mechanism [17, 18] provides possibilities for even lighter axion dark matter masses.

At such a low-energy scale, only Sikivie Haloscopes [19] have reached to the benchmark models of QCD axion dark matter: the Kim-Shifman-Vainshtein-Zakharov (KSVZ) axion [20, 21] and the Dine-Fischler-Srednicki-Zhitnitsky (DFSZ) axion [22, 23]. A Sikivie Haloscope measures axion-to-two-photon coupling $g_{a\gamma\gamma}$ with a resonant cavity in a high magnetic B field. The B field supplies virtual photons to stimulate the conversion of axion dark matter to photons. The photons emitted from the conversion, carrying the total energy of the axion m_a, are confined in the resonant cavity and extracted out by an antenna or lost to the wall. The energy of the axion and the frequency of the photon are interchangeable with the Planck constant in the search.

Currently, the most sensitive axion haloscopes that reach the benchmark model sensitivities lie in the frequency range 0.5 to 1.5 GHz (2 to 6 μeV), including recent results from ADMX [24, 25, 26, 27, 28] and CAPP [29, 30]. In this radio frequency to microwave range, the dominant noise that limits the axion sensitivity is typically Johnson noise of the resonator and the electronic noise of the readout [31]. Natural radioactivities, including alpha, beta, and gamma emissions from primordial radionuclides, deposit energy from keV to MeV and are not a significant contributor to the μeV-to-meV range.

However, the radiation of cosmic-ray muons can induce some physical events that may become noise to axion dark matter searches in a haloscope. Charged particles moving through the magnetic B field can generate cyclotron or synchrotron radiations confined in the resonator, contaminating the axion dark matter search. Since the radiation power is proportional to B^2, the same as the axion signal power, this noise power can be crucial if large enough. To the authors' knowledge, there is no publication on estimating the effects of natural radioactivities and cosmic rays on the axion dark matter haloscopes.

In this manuscript, we explore the synchrotron radiation of cosmic-ray muons at sea level passing through a 8 T uniform solenoid magnetic B field, representing a typical axion haloscope magnetic field. We first use the GEANT4 package [32, 33, 34] to simulate the trajectories of cosmic-ray muons. Due to the non-vertical pitch angle of the cosmic-ray muons to the B field and the non-negligible ratio of the muons with moderate Lorentz factors, $\gamma < 10$, the GEANT4 synchrotron radiation package is inappropriate for our simulation. Therefore, we develop the total synchrotron radiation based on previous analytical work [35, pg. 177-181].

The simulation results show that photons radiated by the cosmic-ray muons are negligible for the current axion haloscope experiments including ADMX and CAPP because of the signal enhancement from the high quality factor Q of the copper cavity resonators and the fine energy resolution in the readout. However, for future broadband axion experiments, such as BREAD [36] and MADMAX [37], if the readout contains photon counters without high enough energy resolution, the synchrotron radiation of cosmic-ray muons might limit the sensitivity.

2 Method

The full simulation can be divided into three steps: cosmic-ray muon generation, trajectory recording and analytical synchrotron radiation integration.

The cosmic-ray muon generator developed in Ref. [38] is integrated into the GEANT4 framework as the particle source. It provides both flat-plane and cylindrical side-wall generations, which simplifies our simulation of cosmic-ray muons entering the bore of a solenoid magnet. We define the region-of-interest to be a copper cavity with 1 m length and 0.2 m radius inside a solenoid magnet bore, which is similar to the facility at ADMX [39]. For such a geometry, we expect a total flux of 17 muons/s going through the top flat surface, and 40 muons/s passing from the side-wall at sea level [38]. We consider these two individual groups of muons separately.

The cosmic-ray muons are generated in the simulation slightly outside this region of interest, being 1 mm away from the outside wall of the copper cavity. The low-energy muons with small bending radius cannot enter the cylindrical cavity and are naturally filtered out. The timestamps of muons entering and leaving the cavity, together with their pitch angles α and Lorentz factors γ are the most important information obtained from the GEANT4 simulation. Figure 1 visualizes 10 trajectories of cosmic-ray muons entering from the top and the wall.

In this work, we estimate the angular-frequency-differential synchrotron radiation power spectra in the cylinder from μeV to meV. Throughout this paper, we report photon energies in eV and muon energies with Lorentz factors γ. We develop our own synchrotron radiation integration based on Ref. [35]. The energy spectrum of cosmic-ray muons at sea level is broad, where 23% are $\gamma < 10$ and 13% are $\gamma > 100$ (Fig. 5). The pitch angles of the muons entering the magnetic field also spread all possibilities from 0° to 90°. A detailed understanding of how the synchrotron radiation changes with different pitch angles is necessary for our calculation.

Here we present more details of the non-trivial synchrotron radiation theories. The total radiation of a charged particle can be calculated following Liénard's formula [40, pg. 664-668]:

$$P = \frac{q^2}{6\pi\epsilon_0 c^3}\gamma^6\left(\dot{\vec{\beta}}^2 - (\vec{\beta}\times\dot{\vec{\beta}})^2\right) = \frac{q^4 B^2 \beta^2 \gamma^2 \sin^2\alpha}{6\pi\epsilon_0 c m^2}, \quad (1)$$

where q and m is the charge and mass of the particle, respectively, $\vec{\beta} = \vec{v}/c$ is the normalized

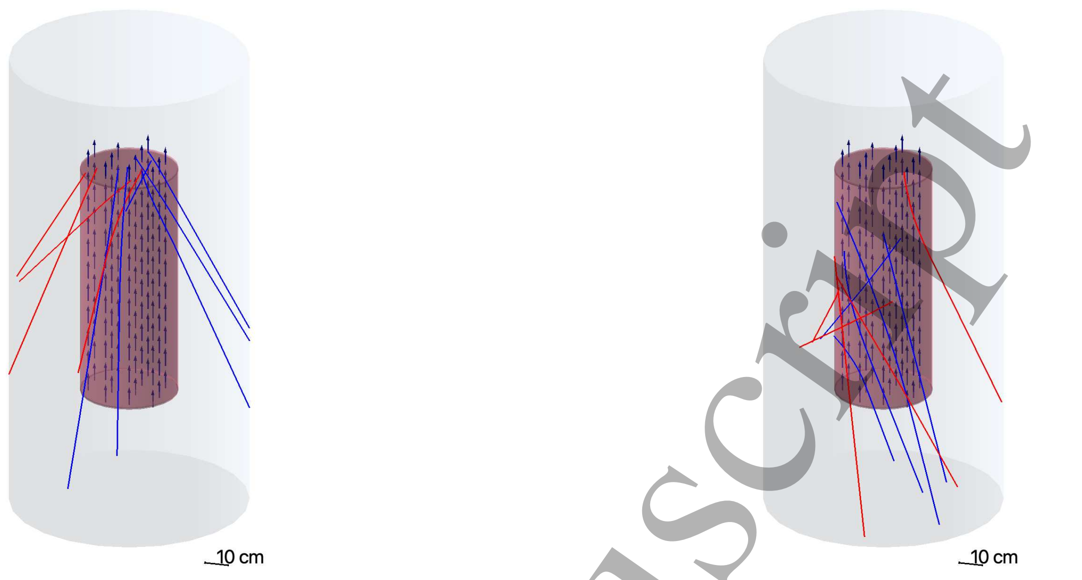

(a) 10 trajectories entering from the top (b) 10 trajectories entering from the wall

Figure 1: Examples of cosmic-ray muon trajectories passing through a copper cavity with GEANT4. Blue and red tracks are μ^+ and μ^-, respectively. An 8 T vertical magnetic field (dark blue arrows) along z-axis is applied to cover the whole copper cylindrical cavity (pink). A larger cylindrical space (grey) is defined to terminate the events.

velocity and α is the pitch angle between $\vec{\beta}$ and $\vec{B}$. SI units are used where ϵ_0 is the vacuum permittivity and c is the speed of light.

The total radiation P in Eq. 1 is used as a sanity check of our numerical integration based on Ref. [35]:

$$P = \frac{q^2\omega_0^2}{8\pi^2\epsilon_0 c}\sum_{n=1}^{\infty}\Big(\int p_n(\alpha,\theta)d\Omega\Big). \tag{2}$$

Here n is harmonic number of the synchrotron radiation, $\omega_0 = qB/m$ is the gyro-angular frequency and $p_n(\alpha,\theta)$ is:

$$p_n(\alpha,\theta) = \frac{n^2\beta_\perp^2(1-\beta^2)}{(1-\beta_\parallel\cos\theta)^3}\Big([J_n'(n\kappa)]^2 + (\frac{\cos\theta-\beta_\parallel}{\beta_\perp\sin\theta})^2[J_n(n\kappa)]^2\Big), \tag{3}$$

where

$$\beta_\perp = \beta\sin\alpha, \quad \beta_\parallel = \beta\cos\alpha,$$
$$\kappa = \frac{\beta_\perp\sin\theta}{1-\beta_\parallel\cos\theta}.$$

J_n and J_n' are the nth order of the Bessel function and its first derivative, respectively. Note that Eq. 3 already integrates the delta function of the allowed frequencies in the synchrotron radiation. The coordinate selections of the lab frame α and θ are shown in figure 2.

The azimuthal symmetry in Eq. 3 reduces the solid angle integral $\int d\Omega$ to a one-dimensional integral over the polar angle θ: $\int d\Omega = \int_0^\pi 2\pi\sin\theta d\theta$. Our numerical integral following Eq. 2 agrees with Eq. 1 at different pitch angles α and Lorentz factors γ.

To calculate the angular-frequency-differential synchrotron radiation power spectrum $dP/d\omega$, we replace the harmonic number n with the angular frequency ω in the lab frame:

$$n = \gamma\omega(1-\beta_\parallel\cos\theta)/\omega_0. \tag{4}$$

When $n \gg 1$ as exemplified in fugure 3a, $dn \approx \gamma(1-\beta_{\parallel\cos\theta})d\omega/\omega_0$ and the direct substitution is appropriate in Eq. 3. However, when n is small, the replacement can cause more than a factor of 3

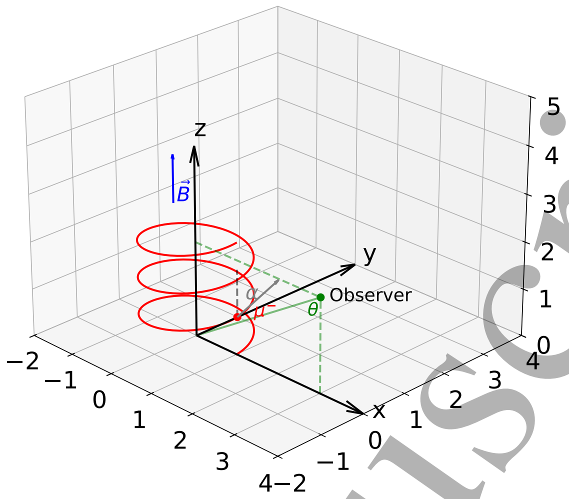

Figure 2: Vector diagram for a muon in helical motion in a uniform magnetic field. Both α and θ are defined in the lab frame.

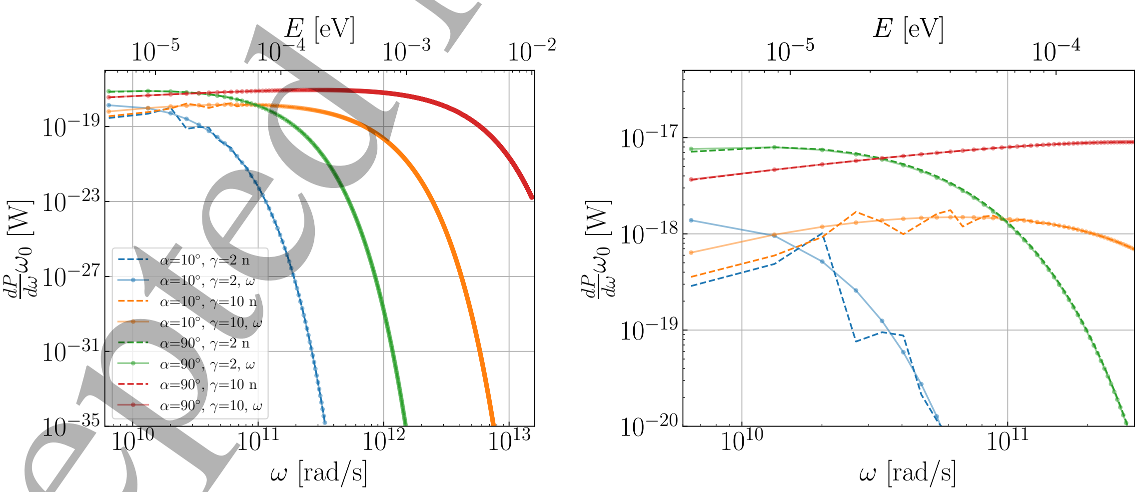

(a) Wide ω range (b) Zoom in on the small ω range

Figure 3: Integrated angular-frequency-differential synchrotron radiation power spectra at different pitch angles α and Lorentz factors γ. The summations with n (dashed lines) agree with substituted ω integrals (dotted lines) when the integration window from ω to $\omega + \omega_0$ spreads a large number of n. The second horizontal x-axis on top converts the angular frequency to energy $E = \hbar\omega$.

deviation since the continuous integral with ω is an average calculation while n can only be integers. The deviation at small n for small γ can be seen in figure 3b.

Therefore, we implement a hybrid calculation for the angular-frequency-differential synchrotron radiation power spectrum $dP/d\omega$. The angular frequencies are binned for the calculation of $dP/d\omega$. For each bin with a lower bound frequency ω_l and an upper bound ω_u. The related boundaries on n are $n_l = \gamma\omega_l(1-\beta_\parallel)/\omega_0$ and $n_u = \gamma\omega_u(1+\beta_\parallel)/\omega_0$. When $n_u - n_l > 100$, we replace n with Eq. 4 directly for the numerical integral. Otherwise, we loop over each n and find the corresponding limits on θ for the integral. Figure 4 illustrates some examples of the angular-frequency-differential synchrotron radiation power spectra with different α and γ. These analytical integrated synchrotron radiation power spectra provide the basic elements of the last step of the simulation. At a specific angular frequency, the averaged synchrotron radiation is normalized based on the cosmic-ray muon events with different γs and αs according to the GEANT4 simulation results.

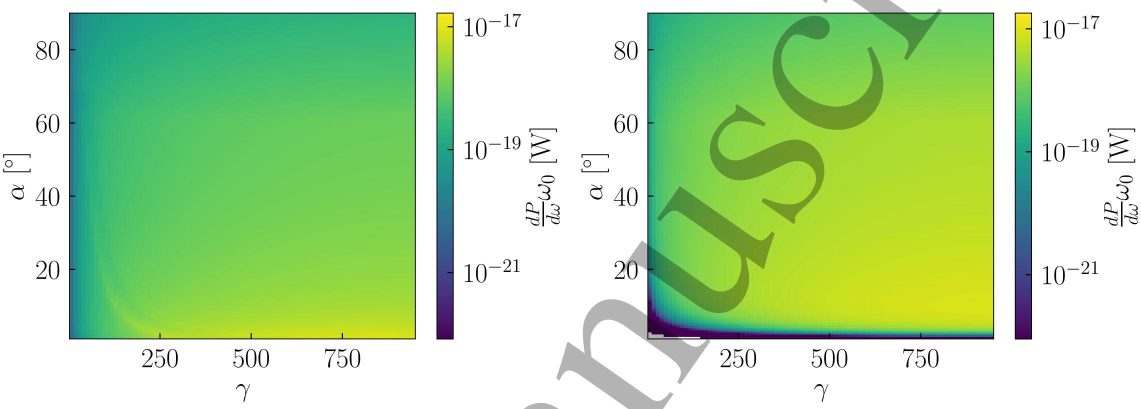

(a) $E = 5 \times 10^{-6}$ eV, $\omega/2\pi = 1.2$ GHz (b) $E = 5 \times 10^{-4}$ eV, $\omega/2\pi = 120.9$ GHz

Figure 4: The angular-frequency-differential synchrotron radiation power spectra at different ωs with the same integral window ω_0 as a function of pitch angle α and Lorentz factor γ.

3 Results

First, we investigate the pitch angle and Lorentz factor distribution of the cosmic-ray muons entering the cylindrical cavity. Figure 5 shows the distributions of the muons entering from the top of the cavity in (a) and the wall of the cavity in (b). Due to more muons entering the cavity from the wall, the synchrotron radiation power of the wall muon group is more significant. Note, a lower boundary of $\gamma > 2$ was implemented for the simulated muon generator, corresponding to the momentum $p > 0.1$ GeV. This is the valid minimum momentum of the cosmic-ray muon generator that agrees with the experimental data in Ref. [38].

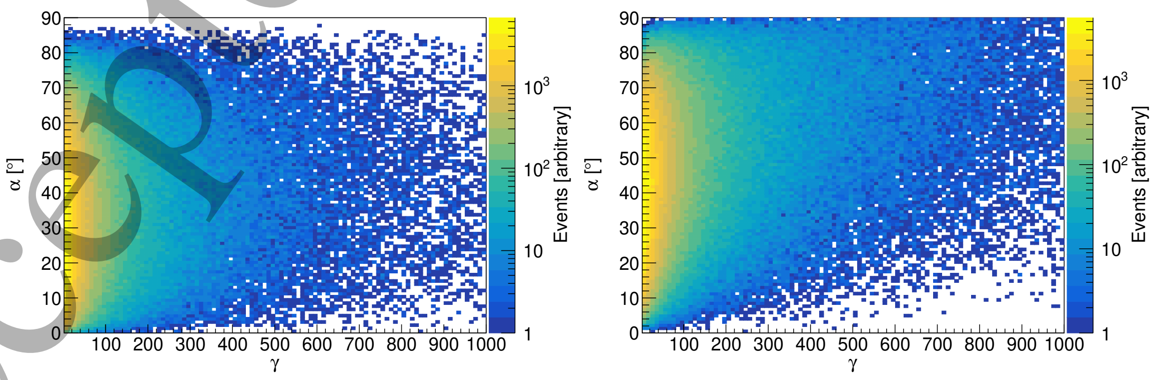

(a) Top (b) Wall

Figure 5: Pitch angle α and Lorentz factor distributions γ of cosmic-ray muons at sea level

.

Figure 6 illustrates the time muons stay in the region of interest for both the top and wall groups. Most of the muons stay in the 1 m long cylindrical space for several nanoseconds, which agrees with the speed of light estimation. Interestingly, there is a tail feature in the α-time distribution for muons entering from the top with a residence time in the cavity > 3.2 ns and $\alpha < 70°$. Further investigation shows that these events are more mildly relativistic with $\gamma < 10$, and the cyclotron radius is smaller than the radius of the cavity (0.2 m). They stay longer in the cavity with helical motions as exemplified in figure 2.

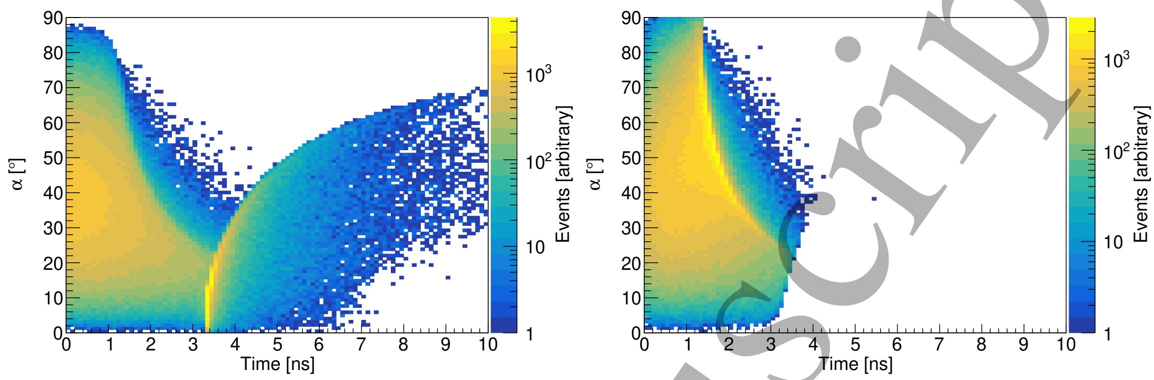

(a) Top (b) Wall

Figure 6: Distribution of the muon time in the copper cavity with different pitch angles α
.

We focus on the synchrotron radiation from the cosmic-ray muons between 4 μeV and 10 meV. This energy range covers most of the well-motivated energy range for post-inflation QCD axion dark matter. The gyro-angular frequency of a non-relativistic muon in 8 T is $\omega_0 = 6.8 \times 10^9$ rad/s, which is taken as the start of the angular-frequency-differential synchrotron radiation power spectrum as well as the step in the spectrum. Correspondingly, the energy step size is $\delta E = \hbar\omega_0 = 4.4$ μeV.

The angular-frequency-differential synchrotron radiation power spectra for different α and γ are calculated separately. In the frame where the muon undergoes circular motion, synchrotron radiation can only be emitted at specific frequencies, $n\omega_0$, corresponding to different harmonic numbers n. To visualize the differential synchrotron radiation spectra, we use $\frac{dP}{d\omega}\omega_0$ to present the averaged differential synchrotron radiation over each ω_0 integral window. Figure 4 presents two examples of the differential synchrotron radiation spectra at 5 μeV and 0.5 meV as a function of the pitch angle α and Lorentz factor γ.

The averaged synchrotron radiation power spectra density of the cosmic-ray muons over different α and γ at sea level are shown in figure 7. We converted the angular frequency ω to frequency $f = \omega/2\pi$ since the latter is more commonly used in the axion haloscope community. We have scaled the spectra with the expected muon rates: 17 muons/s for the top and 40 muons/s for the wall. The difference in the muon rates dominates the contribution of the synchrotron radiation. Both the top and the wall present broad radiation, spreading from μeV to meV with the synchrotron radiation power on the same order.

The uncertainties in our estimation of cosmic-ray muon synchrotron radiation can come from three different parts: (1) the cosmic-ray muon flux parametrization; (2) the possible muon deflection before reaching the sensitive region and (3) the numerical integration of the synchrotron radiation formula. Most of the cosmic-ray muons ($\sim$90%) have small pitch angles $< 10°$, which have the flux parametrization accurate within a few percent in Ref. [38], making the muon flux uncertainty minor (smaller than 10%). The binding radius for these muons are typically larger than 10 m, so the deflection before reaching the sensitive range is also a minor effect. The last factor will contribute the most for photon energy $E < 10^{-4}$ eV (Fig. 3). Because the muon radiation is at discrete frequencies in the frame with the muon moving circularly. The effect can dramatically vary from one frequency to another, depending on whether the muon radiation harmonics share the same frequencies with the axion searches. For real experiments that are affected by cosmic-ray muon synchrotron radiation, the uncertainties should be considered carefully.

To explain how the muon synchrotron radiation can affect axion dark matter detection, we compare the muon synchrotron noise power to the microwave signal power from the axion-to-photon conversion of a Sikivie haloscope [19, 39]. The microwave signal power generated

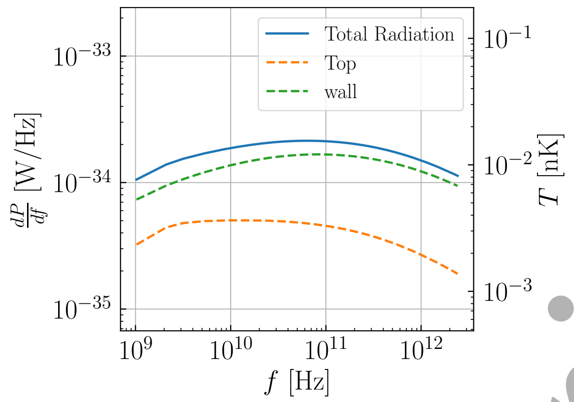

Figure 7: The averaged power spectrum density (blue solid line) of the cosmic-ray muons. The contributions of the top muons (orange dashed line) and the wall (green dashed line) are scaled with the expected rates at the sea level. The y-axis on the right-hand side converts the energy into noise temperature $T = \frac{dP}{df} \cdot \frac{1}{k_B}$, where k_B is the Boltzmann constant.

inside a haloscope is:

$$P_{\rm a} = 1.0 \times 10^{-27}\ {\rm W} \left(\frac{V_{\rm eff}}{50\ \ell}\right) \left(\frac{B}{8\ {\rm T}}\right)^2 \left(\frac{g_\gamma}{0.36}\right)^2 \left(\frac{\rho_a}{0.45\ {\rm GeV/cc}}\right) \left(\frac{f}{1\ {\rm GHz}}\right) Q. \quad (5)$$

Here $V_{\rm eff}$ is the effective volume that accounts for the overlap efficiency between the external $\vec{B}$ field and the cavity's electric field mode at the resonant frequency f. When the axion dark matter (with local density $\rho_a \sim$0.45 GeV [41, 42]) is on resonance with the cavity, the signal power is enhanced by the quality factor Q. As a concrete example, for the ADMX experiment at 1 GHz with the copper cavity on resonance, Q can typically reach 50,000. The g_γ is the model-dependent dimensionless coefficient: the KSVZ axion has $g_\gamma = -0.97$ [20, 21] and the more feebly coupled DFSZ axion has $g_\gamma = 0.36$ [22, 23].

In figure 8a, DFSZ axion power is calculated with $V_{\rm eff} = 50\ \ell$ and different Qs. The muon synchrotron radiation power is calculated based on the averaged power spectra density in figure 7 and different assumed relative energy resolutions $\Delta E/E$. When $\Delta E/E = 10\%$, the muon contribution is comparable to the DFSZ axion signal power at $Q = 10$. Figure 8b further illustrates the Q for different energy resolutions if $P_a = P_{\rm axion}$, which indicates the minimum Q requirements. For worse energy resolution, the effective frequency span in our calculation is smaller. The noise power of the muons' synchrotron radiation is trivial for experiments such as ADMX on $\mathcal{O}(1)$ μeV. However, when low energy resolution photon detectors are used and lower Q is designed for broader detection band, the cosmic-ray muon synchrotron radiation is likely to be a source of non-negligible noise power.

4 Discussion and Conclusion

Cosmic-ray muons are only one type of natural events that bring broadband microwave radiation. Secondary charged particles excited by the muons and beta decays have similar effects for axion haloscopes. Especially, the delta electrons generated on the inner surface of the detector with energy higher than 100 MeV can radiate photons spreading μeV to meV as well. Even if the rate of high-energy delta electrons is lower than the muons, but each electron radiates 4×10^4 more total radiation power (due to the mass difference) compared to muons with the same conditions according to the Liénard's formula. The relativistic electrons can increase the requirements on the energy resolution and the signal enhancement by several orders for broadband experiments, which we plan to investigate in future works.

We only compare the initial synchrotron radiation and signal power inside the cavity. Some detector designs, including BREAD and MADMAX, will only collect the synchrotron radiation with some specific polarizations. The methodology can be adapted to different experiments according to Eq. 2 and 3 for estimating the synchrotron radiation effects of charged particles.

The design of a Sikivie haloscope can be used for high-frequency gravitation wave searches directly [43]. Similar designs can also be found in the beta decay measurements using cyclotron radiation emission spectroscopy [44, 45]. The considerations discussed in this work should therefore be taken into account in the planning and design of these future experiments as well.

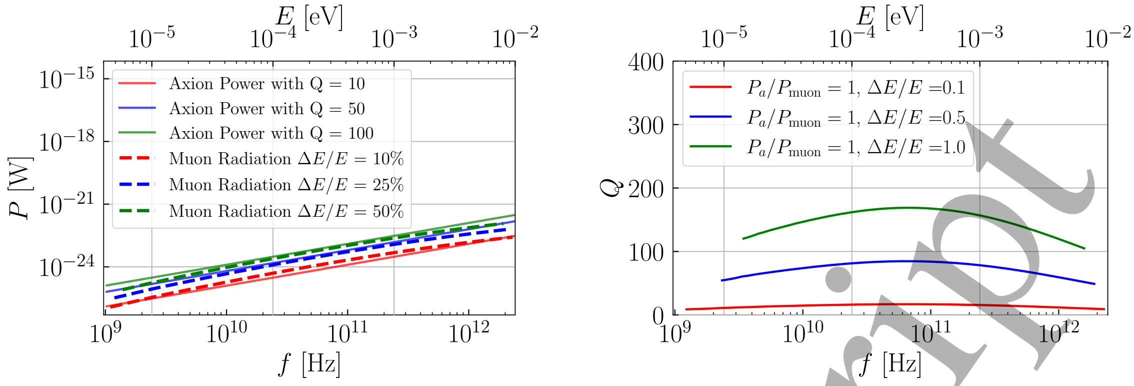

(a) Power Spectra

(b) Axion VS Muon Power

Figure 8: (a) The axion power P_a with different enhancements Q (solid lines) compared to muon synchrotron radiation with different energy resolutions (dashed lines). Here typical parameters close to the ADMX experiments are used in the P_a calculations [39]. (b) The Qs leading to $P_a = P_{\text{axion}}$ at different energy resolutions.

In brief, we study the possible noise power coming from cosmic-ray muons for axion dark matter searches between 4 μeV and 10 meV. We explain that cosmic-ray muons are negligible in the current experiments using axion haloscopes for the signal enhancement with a high quality factor Q and fine energy resolution of the readout. Furthermore, we note that broadband designs utilizing photon counters can be compromised by the cosmic-ray muons and natural radioactivities, particularly without sufficient signal enhancement or adequate energy resolution.

Acknowledgements
We thank the University of Washington Research Award from the Global Innovation Fund to support the collaboration of this work.

References

[1] Aghanim, N. et al. Planck 2018 results - vi. cosmological parameters. *A&A*, 641:A6, 2020.

[2] G. 't Hooft. Symmetry breaking through bell-jackiw anomalies. *Phys. Rev. Lett.*, 37:8–11, Jul 1976.

[3] P. D. Miller, W. B. Dress, J. K. Baird, and Norman F. Ramsey. Limit to the electric dipole moment of the neutron. *Phys. Rev. Lett.*, 19:381–384, Aug 1967.

[4] C. Abel et al. Measurement of the permanent electric dipole moment of the neutron. *Phys. Rev. Lett.*, 124:081803, Feb 2020.

[5] R. D. Peccei and Helen R. Quinn. CP conservation in the presence of pseudoparticles. *Phys. Rev. Lett.*, 38:1440–1443, Jun 1977.

[6] Steven Weinberg. A New Light Boson? *Phys. Rev. Lett.*, 40:223–226, 1978.

[7] Frank Wilczek. Problem of Strong p and t Invariance in the Presence of Instantons. *Phys. Rev. Lett.*, 40:279–282, 1978.

[8] J. Ipser and P. Sikivie. Can galactic halos be made of axions? *Phys. Rev. Lett.*, 50:925–927, Mar 1983.

[9] John Preskill, Mark B. Wise, and Frank Wilczek. Cosmology of the invisible axion. *Physics Letters B*, 120(1):127–132, 1983.

[10] Michael Dine and Willy Fischler. The not-so-harmless axion. *Physics Letters B*, 120(1):137–141, 1983.

[11] William A. Bardeen and S.-H.H. Tye. Current algebra applied to properties of the light higgs boson. *Physics Letters B*, 74(3):229–232, 1978.

[12] T. W. Donnelly, S. J. Freedman, R. S. Lytel, et al. Do axions exist? *Phys. Rev. D*, 18:1607–1620, Sep 1978.

[13] Matthew J. Dolan, Frederick J. Hiskens, and Raymond R. Volkas. Advancing globular cluster constraints on the axion-photon coupling. *Journal of Cosmology and Astroparticle Physics*, 2022(10):096, oct 2022.

[14] Andrea Caputo and Georg Raffelt. Astrophysical Axion Bounds: The 2024 Edition. *PoS*, COSMICWISPers:041, 2024.

[15] Vincent B. Klaer and Guy D. Moore. The dark-matter axion mass. *JCAP*, 11:049, 2017.

[16] Marco Gorghetto, Edward Hardy, and Giovanni Villadoro. More axions from strings. *SciPost Phys.*, 10:050, 2021.

[17] Peter W. Graham and Adam Scherlis. Stochastic axion scenario. *Phys. Rev. D*, 98:035017, Aug 2018.

[18] Fuminobu Takahashi, Wen Yin, and Alan H. Guth. Qcd axion window and low-scale inflation. *Phys. Rev. D*, 98:015042, Jul 2018.

[19] P. Sikivie. Experimental tests of the "invisible" axion. *Phys. Rev. Lett.*, 51:1415–1417, Oct 1983.

[20] Jihn E. Kim. Weak Interaction Singlet and Strong CP Invariance. *Phys. Rev. Lett.*, 43:103, 1979.

[21] Mikhail A. Shifman, A.I. Vainshtein, and Valentin I. Zakharov. Can Confinement Ensure Natural CP Invariance of Strong Interactions? *Nucl.Phys.*, B166:493, 1980.

[22] Michael Dine, Willy Fischler, and Mark Srednicki. A Simple Solution to the Strong CP Problem with a Harmless Axion. *Phys. Lett.*, B104:199, 1981.

[23] A.R. Zhitnitsky. On Possible Suppression of the Axion Hadron Interactions. (In Russian). *Sov. J. Nucl. Phys.*, 31:260, 1980.

[24] N. Du, N. Force, R. Khatiwada, et al. Search for invisible axion dark matter with the axion dark matter experiment. *Phys. Rev. Lett.*, 120:151301, Apr 2018.

[25] T. Braine, R. Cervantes, N. Crisosto, et al. Extended search for the invisible axion with the axion dark matter experiment. *Phys. Rev. Lett.*, 124:101303, Mar 2020.

[26] C. Bartram, T. Braine, E. Burns, et al. Search for invisible axion dark matter in the $3.3 - -4.2$ μeV mass range. *Phys. Rev. Lett.*, 127:261803, Dec 2021.

[27] C. Goodman, M. Guzzetti, C. Hanretty, et al. Admx axion dark matter bounds around 3.3 μeV with dine-fischler-srednicki-zhitnitsky discovery ability. *Phys. Rev. Lett.*, 134:111002, Mar 2025.

[28] G. Carosi, C. Cisneros, N. Du, et al. Search for axion dark matter from 1.1 to 1.3 ghz with admx. *Phys. Rev. Lett.*, 135:191001, Nov 2025.

[29] Andrew K. Yi, Saebyeok Ahn, Ça ğlar Kutlu, et al. Axion dark matter search around 4.55 μeV with dine-fischler-srednicki-zhitnitskii sensitivity. *Phys. Rev. Lett.*, 130:071002, Feb 2023.

[30] Saebyeok Ahn, JinMyeong Kim, Boris I. Ivanov, et al. Extensive search for axion dark matter over 1 ghz with capp's main axion experiment. *Phys. Rev. X*, 14:031023, Aug 2024.

[31] M. Guzzetti, D. Zhang, C. Goodman, et al. Improved receiver noise calibration for admx axion search: 4.54 to 5.41 μev. *Phys. Rev. D*, 111:092012, May 2025.

[32] J. Allison, K. Amako, J. Apostolakis, et al. Recent developments in geant4. *Nuclear Instruments and Methods in Physics Research Section A: Accelerators, Spectrometers, Detectors and Associated Equipment*, 835:186–225, 2016.

[33] J. Allison, K. Amako, J. Apostolakis, et al. Geant4 developments and applications. *IEEE Transactions on Nuclear Science*, 53(1):270–278, 2006.

[34] S. Agostinelli, J. Allison, K. Amako, J. Apostolakis, et al. Geant4—a simulation toolkit. *Nuclear Instruments and Methods in Physics Research Section A: Accelerators, Spectrometers, Detectors and Associated Equipment*, 506(3):250–303, 2003.

[35] G. BEKEFI. *Radiation Processes In Plasmas*. JOHN WILEY AND SONS, 1966.

[36] Gabe Hoshino, Stefan Knirck, Mohamed H. Awida, et al. First axionlike particle results from a broadband search for wavelike dark matter in the 44 to 52 μeV range with a coaxial dish antenna. *Phys. Rev. Lett.*, 134:171002, Apr 2025.

[37] B. Ary dos Santos Garcia, D. Bergermann, A. Caldwell, et al. First search for axion dark matter with a madmax prototype. *Phys. Rev. Lett.*, 135:041001, Jul 2025.

[38] D. Pagano, G. Bonomi, A. Donzella, A. Zenoni, et al. Ecomug: An efficient cosmic muon generator for cosmic-ray muon applications. *Nuclear Instruments and Methods in Physics Research Section A: Accelerators, Spectrometers, Detectors and Associated Equipment*, 1014:165732, 2021.

[39] R. Khatiwada, D. Bowring, A. S. Chou, et al. Axion dark matter experiment: Detailed design and operations. *Review of Scientific Instruments*, 92(12):124502, 12 2021.

[40] J. D. Jackson. *Classical Electrodynamics*. Wiley, 3rd edition, 1999.

[41] Evalyn I. Gates, Geza Gyuk, and Michael S. Turner. The local halo density. *The Astrophysical Journal*, 449(2):L123, aug 1995.

[42] Pablo F de Salas and A Widmark. Dark matter local density determination: recent observations and future prospects. *Reports on Progress in Physics*, 84(10):104901, oct 2021.

[43] Kristof Schmieden and Matthias Schott. The global network of cavities to search for gravitational waves (gravnet): A novel scheme to hunt gravitational waves signatures from the early universe, 2023. arXiv:2308.11497.

[44] A. Ashtari Esfahani, S. Bhagvati, S. Böser, M. J. Brandsema, et al. Antenna arrays for neutrino mass measurements with cyclotron radiation emission spectroscopy. *Phys. Rev. C*, 112:045506, Oct 2025.

[45] N. Buzinsky et al. Larmor power limit for cyclotron radiation of relativistic particles in a waveguide. *New J. Phys.*, 26(8):083021, 2024.